

A Passive Satellite Deorbiting Strategy for MEO Using Solar Radiation Pressure and the J_2 Effect

Charlotte Lücking*, Camilla Colombo, and Colin R. McInnes
Advanced Space Concepts Laboratory, University of Strathclyde
Glasgow, G1 1XJ, United Kingdom

The growing population of space debris poses a serious risk to the future of space flight. To effectively manage the increase of debris in orbit, end-of life disposal has become a key requirement for future missions. This poses a challenge for Medium Earth Orbit (MEO) spacecraft which require a large Δv to re-enter the atmosphere or reach the geostationary graveyard orbit. This paper further explores a passive strategy based on the joint effects of solar radiation pressure and the Earth's oblateness acting on a high area-to-mass ratio object. The concept was previously presented as an analytical planar model. This paper uses a full 3D model to validate the analytical results numerically for equatorial circular orbits first, then investigating higher inclinations. It is shown that for higher inclinations the initial position of the Sun and right ascension of the ascending node become increasingly important. A region of very low required area-to-mass ratio is identified in the parameter space of a and inclination which occurs for altitudes below 10,000 km.

NOTATION

| | | | |
|-------------|--|-------------------|--|
| a | semi-major axis [m] | λ_{\odot} | angle of position of the Sun on ecliptic with respect to the vernal equinox [rad] |
| a_{SRP} | acceleration by solar radiation pressure [m/s^2] | μ | gravitational parameter of the Earth |
| c | speed of light in vacuum [m/s] | ω | argument of perigee [rad] |
| c_R | coefficient of reflectivity | Ω | right ascension of the ascending node [rad] |
| e | eccentricity | ϕ | angle between the direction of the solar radiation and the radius of the perigee [rad] |
| e_{crit} | critical eccentricity | σ | area-to-mass ratio [m^2/kg] |
| f | true anomaly [rad] | | |
| F_{\odot} | solar flux [W/m^2] | | |
| H | Hamiltonian | | |
| i | inclination [rad] | | |
| J_2 | second order zonal harmonic coefficient of the Earth | | |
| n_{\odot} | rotational rate of the Earth around the Sun [rad/s] | | |
| R_E | radius of the Earth [m] | | |
| α | solar radiation pressure parameter | | |
| κ | J_2 effect parameter | | |

1. INTRODUCTION

In 1993 the Inter-Agency Space Debris Coordination Committee was formed and issued guidelines for the mitigation of space debris which demands a removal of any spacecraft from certain protected regions within 25 years after the end of operations [1]. These protected regions are currently defined as Low Earth Orbit (LEO) and Geostationary Earth Orbit (GEO). Although the region in between, Medium Earth Orbit (MEO) is not currently a protected region, the implementation of an end-of-life strategy is also encouraged for MEO [2]. In particular the area in which Global Navigation Satellite

* charlotte.lucking@strath.ac.uk

Systems (GNSS) spacecraft can be found, such as GLONASS, NavStar GPS and future Galileo and Beidou satellites, is deemed worthy of a special status. A recent European commission report estimates that 6-7% of the GDP of developed countries is dependent on satellite navigation [3]. That is around \$1 trillion in Europe alone.

GNSS constellations are located in upper MEO at altitudes between 18,000 km and 24,000 km. Lower MEO with altitudes up to 5,000 km could be a region of future interest for small satellite missions. This regime offers a larger field of view and longer pass times than LEO while still remaining within a distance from the Earth which allows good resolution remote sensing and low latency communications. However, at this altitude the effect of drag is negligible and any spacecraft placed there would remain in orbit indefinitely unless an end-of-life strategy is applied. This is a problem particularly for small satellites because they are built with strict cost constraints and thus rarely feature a propulsion system capable of large orbital manoeuvres.

Passive deorbiting technologies which have previously been suggested either make use of the aerodynamic [4-7] or the electrodynamic drag force [8-10]. Both effects decrease rapidly with increasing distance from the Earth and are not feasible for exploitation in MEO. Previous research has shown that solar radiation pressure coupled with the Earth's oblateness can have a significant effect on the evolution of MEO spacecraft with an artificially increased area-to-mass ratio and that this effect is strong enough to be used for deorbiting [11, 12]. After the deployment of a light-weight reflective structure to increase the surface area, the manoeuvre requires no further control inputs and the spacecraft deorbits passively. An analytical solution has been derived for planar orbits.

In this paper these analytical results are verified numerically by using a full 3D model [13]. First, objects tracked by NORAD are analysed to determine the most important orbital regions within MEO and the future potential of MEO missions. Then a summary of the analytical method and results in [11] and [12] is given. Next the analytical results are verified for equatorial orbits in a three-dimensional numerical model. The strategy is also tested numerically for circular and eccentric inclined orbits.

2. SURVEY OF MEO OBJECTS

Medium Earth Orbit (MEO) is defined as a regime of orbits with altitudes between Low Earth Orbit (LEO) and the geostationary ring. This means the regime between 2,000 km and 35,586 km altitude. In this section only orbits which lie entirely in the MEO region are considered i.e. all orbits with a perigee altitude above 2,000 km and an apogee altitude of less than 35,586 km, the upper boundary of LEO and lower boundary of GEO respectively. There are 546 tracked objects in the NORAD database¹ which fulfil these requirements. Just 12 of them have meanwhile decayed. All others are still in their orbits although only 56 are categorised as operational. In the population of MEO six distinctive groups of spacecraft can be identified which make up 85% of the total MEO spacecraft population:

- ▶ GLONASS, the Russian satellite navigation system can be found in quasi circular orbits with just below 20,000 km altitude.
- ▶ NavStar, the American GPS satellites occupy quasi circular orbits with altitudes just above 20,000 km.
- ▶ The Initial Defence Satellite Communications System (IDSCS) was the precursor constellation to the American Defence Satellite Communications System (DSCS) and launched in the late 1960s into circular orbits with altitudes below GEO to give contact times of up to four days.
- ▶ Oko is the Russian defence constellation for early warning. It was launched over forty years into Molniya orbits with 600 km perigee altitude and 63.7 degrees of inclination. The Oko spacecraft appearing in this survey have drifted from their orbit gaining perigee altitude to now lie entirely within the MEO [14].

¹ <http://celestrak.com/> Retrieved on 05 Sep 2011

- ▶ The future GNSS constellations: Galileo is the European satellite navigation system and is likely to make up a large part of total MEO launches in future. So far only two precursor satellites, GIOVE A and B, have been launched. They occupy future Galileo orbits which are circular, inclined and at an altitude of around 23,000 km. Beidou is the future Chinese satellite navigation constellation in MEO and GEO. One MEO satellite has been launched so far in 2007. Beidou will occupy circular, inclined orbits in around 21,500 km altitude.
- ▶ The West Ford needle experiment is not strictly a satellite constellation. In the 1960s thousands of small metal needles were launched into high altitude polar orbits in a bid to improve long-range HF radio communications. Although some of these needles have meanwhile re-entered the atmosphere, large numbers still remain in their orbits as space debris [15].

Figure 1 shows the number and type of launches into MEO per half decade. It can be seen that most of the MEO constellations have been stocked over long periods of time with Galileo and Beidou only just beginning. There was large interest in MEO in the late 1960s but apart from that not a lot of activity until the 1980s. The satellite navigation constellations have made up the largest part of MEO launches in the last thirty years.

Figure 2 shows the inclination and altitude of the different space object groups with tracked space debris and rocket bodies shown in light grey in the background. The perigee and apogee altitudes of the spacecraft are marked with a filled circle. The eccentricity of a spacecraft’s orbit can be seen by the distance between perigee and apogee. While circular orbits appear as just one point, eccentric orbits are long lines connecting the perigee and apogee. It can be seen that main orbits of interest are circular GNS-like orbits with altitudes around 20,000 km and inclinations between 50 and 70 degrees and highly eccentric Molniya-type orbits with high inclinations of 60 to 70 degrees and semi-major axes of around 30,000 km.

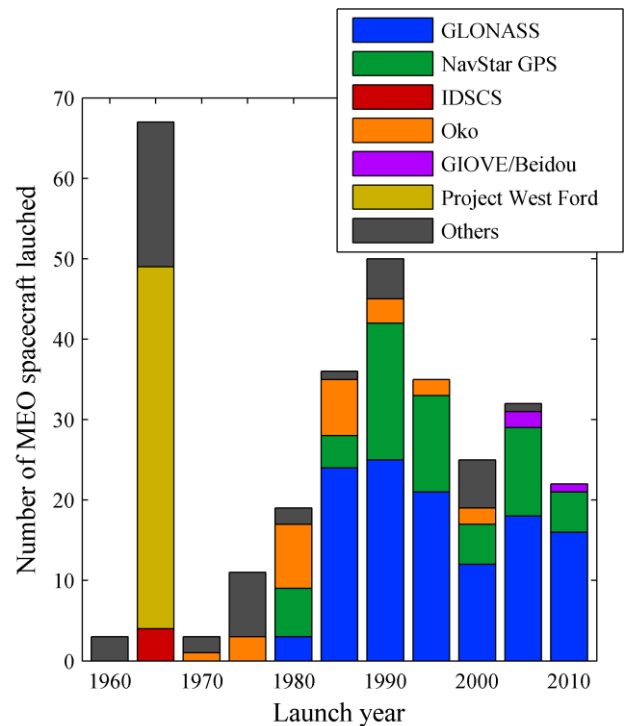


Figure 1: Number of MEO objects launched by date and category.

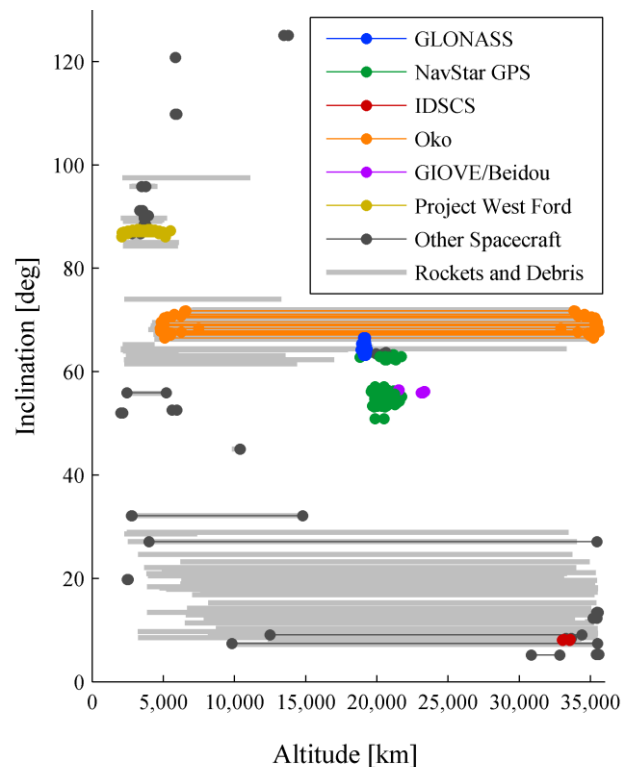


Figure 2: Objects currently in MEO by category on a graph of inclination and altitude. Perigee and apogee altitude of spacecraft and Westford needles are marked with a circle.

3. ANALYTICAL PLANAR MODEL

We consider the orbit in a rotational reference frame that follows the Earth around the Sun. In this frame three parameters are needed to define any in-plane orbit. The eccentricity e , semi-major axis a and the angle between the direction of the solar radiation and the radius of the perigee with respect to the Earth, ϕ . Figure 3 shows the geometry of the rotational reference frame.

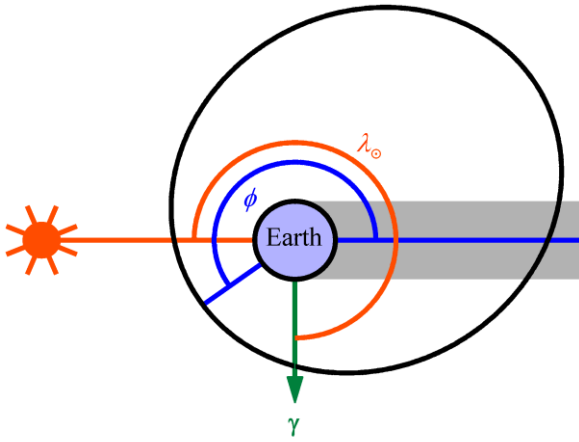


Figure 3: Planar Earth orbit in rotating reference frame.

Krivov and Getino's work on the orbital dynamics of high area-to-mass ratio spacecraft introduces an approximate Hamiltonian for planar orbits under the effects of solar radiation pressure and the Earth's oblateness [16]:

$$H = -\sqrt{1-e^2} + \alpha e \cos \phi - \frac{\kappa}{3\sqrt{1-e^2}^3} \quad (1)$$

α is a parameter related to the influence of solar radiation pressure on the orbit and κ is related to the J_2 effect:

$$\alpha = \frac{3}{2n_\odot} a_{SRP} \sqrt{\frac{a}{\mu}} \quad (2)$$

$$\kappa = \frac{3}{2n_\odot} J_2 R_E^2 \sqrt{\frac{\mu}{a^7}} \quad (3)$$

where a_{SRP} is the acceleration the spacecraft experiences due to solar radiation pressure and can be calculated as:

$$a_{SRP} = \frac{F_\odot}{c} c_R \sigma \quad (4)$$

F_\odot is the solar radiation flux at Earth, c is the speed of light in vacuum. The defining spacecraft characteristic is the effective area-to-mass ratio $c_R \sigma$, the product of c_R , the coefficient of reflectivity, and σ , the area-to-mass ratio. The coefficient of reflectivity depends on the optical properties for the device and its geometry. For a flat, highly reflective surface facing the Sun $c_R \approx 2$. This model does not consider eclipses or the tilt of the Earth's rotational axis with respect to the ecliptic plane. As a consequence, the semi-major axis remains constant and the evolution of the orbit can be described only by its eccentricity e and solar radiation – perigee – angle ϕ . Initially circular orbits will librate around an equilibrium in the phase space which is either perigee Sun-pointing, e_π , or apogee Sun-pointing, e_0 . Around which equilibrium the libration takes place depends on the semi-major axis and the area-to-mass ratio of the spacecraft [12, 13].

In order to calculate the area-to-mass ratio needed to reach the required eccentricity for deorbiting, the following analytic expressions were derived in [11]:

$$\alpha_{\phi=0} = \frac{1-\sqrt{1-e^{*2}}}{e^*} + \left(\frac{1}{3e^*} - \frac{1}{3e^* \sqrt{1-e^{*2}{}^3}} \right) \kappa \quad (5)$$

$$\alpha_{\phi=\pi} = - \left(\frac{1-\sqrt{1-e^{*2}}}{e^*} + \left(\frac{1}{3e^*} - \frac{1}{3e^* \sqrt{1-e^{*2}{}^3}} \right) \kappa \right) \quad (6)$$

Eq. (5) gives the minimum required solar radiation parameter for deorbiting for a libration around the e_0 equilibrium and the maximum eccentricity is reached when the apogee is Sun-pointing. Figure 4 visualises the Hamiltonian in the orbital element phase space of eccentricity and orientation for a spacecraft with semi-major axis of 10,000 km and the minimum solar radiation parameter α_0 to deorbit from an initially circular orbit. The initial orbit is on the x-axis with $e=0$ and then follows the purple phase line until the critical eccentricity is reached at $\phi=0$. The critical eccentricity, e_{crit} , is the eccentricity at which the perigee altitude is 0 km and can be calculated as:

$$e_{crit} = 1 - \frac{R_E}{a} \quad (7)$$

where R_E is the radius of the Earth and a is the semi-major axis. In the figure the e_0 equilibrium is marked by a purple circle and it can be clearly seen that the deorbiting manoeuvre follows the libration behaviour around it.

Eq. (6) is for a manoeuvre following the libration around the other equilibrium, e_π , at $\phi = \pi$ which appears only for larger semi-major axes. The maximum eccentricity is reached when the perigee is Sun-pointing. Figure 5 shows the orbital element phase space for a semi-major axis of 20,000 km and the minimum solar radiation parameter α_π to deorbit. The e_π equilibrium is marked in blue and a blue line traces the evolution of an initially circular orbit.

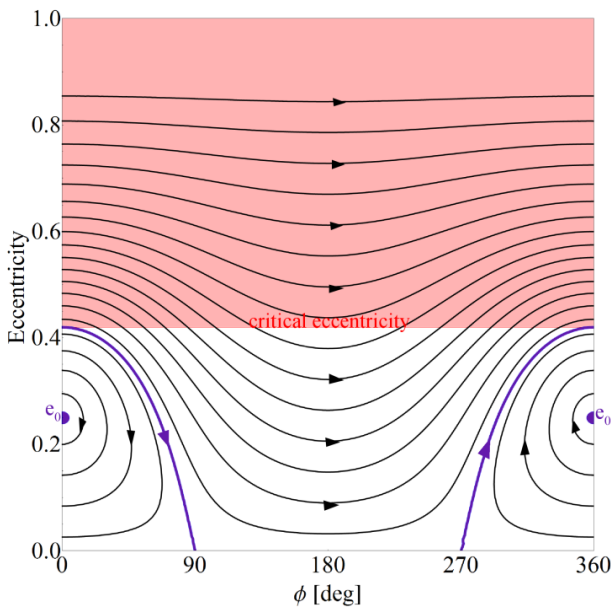


Figure 4: Orbital element phase space for planar orbits with 10,000 km semi-major axis for a spacecraft with required area-to-mass ratio to deorbit an initially circular orbit.

From the required solar radiation parameter for deorbit (Eqs. (5) and (6)) the effective area-to-mass ratios after the deployment of the deorbiting device can be calculated using Eqs. (2) and (4). Figure 7 shows the resulting effective area-to-mass ratios as a function of semi-major axis. The minimum at about 7,500 km altitude occurs when the altitude is between the two behaviour regimes shown in Figure 4 and Figure 5. The evolution then first follows a libration around e_π . Then it changes direction, librating around e_0 before

reaching the critical eccentricity at $\phi = 0$. This way the orbit remains longer in the regime of $\pi < \phi < 2\pi$ where the derivative of the eccentricity is positive. Figure 6 shows the orbital element phase space in this regime. The e_π equilibrium is marked in blue and the e_0 equilibrium in purple. The evolution of an initially circular orbit is traced in blue and purple depending on the direction of its evolution in ϕ .

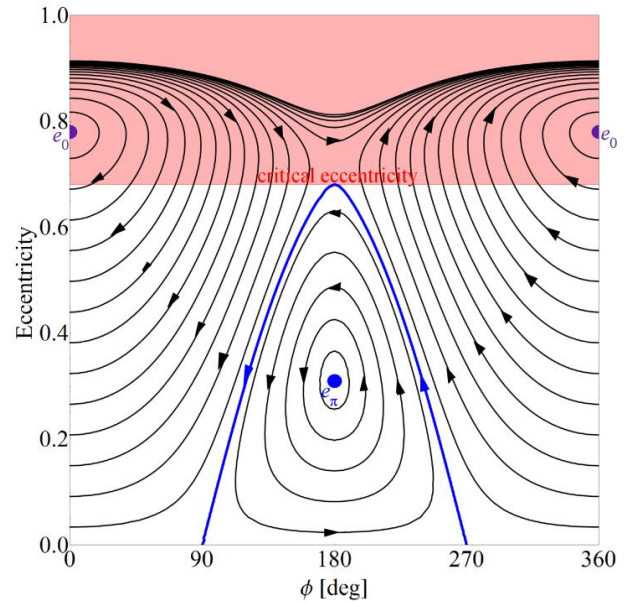


Figure 5: Orbital element phase space for planar orbits with 20,000 km semi-major axis for a spacecraft with required area-to-mass ratio to deorbit an initially circular orbit.

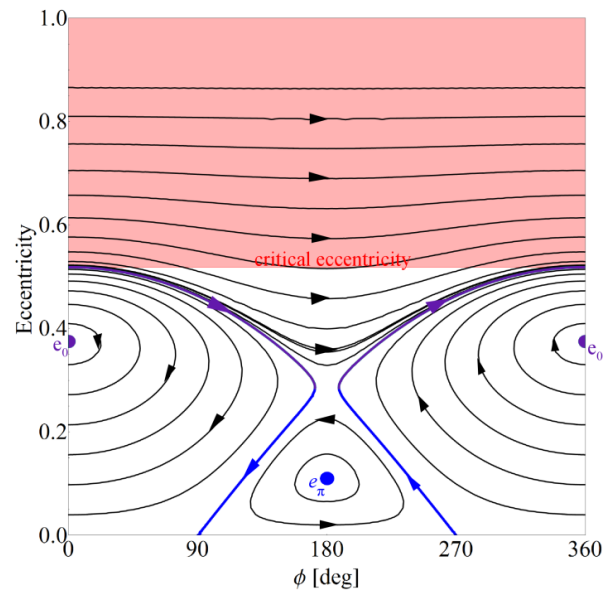


Figure 6: Orbital element phase space for planar orbits with 13,250 km semi-major axis for a spacecraft with required effective area-to-mass ratio to deorbit an initially circular orbit.

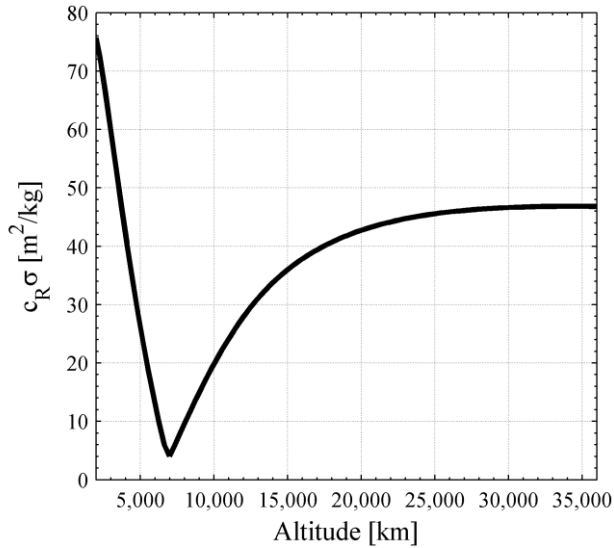


Figure 7: Analytical results for the required effective area-to-mass ratio to deorbit.

4. NUMERICAL 3D MODEL

In this section the analytical theory presented in [11] and [12] and summarised in the previous section will be numerically verified for equatorial orbits in a three-dimensional reference frame and tested for inclined orbits. A general investigation of the 3D orbital element phase space under the influence of solar radiation pressure and J_2 can be found in [13].

4.1. Numerical model and propagation

In the 3D model the actual obliquity angle of the ecliptic with respect to the Earth equator is considered. The orbital dynamics are propagated by numerically integrating the Gauss' equations in non-singular Lagrangian elements [17]. The use of those equations for inclined orbits has been analysed in [13]. The numerical propagation considers only the perturbations of solar radiation pressure and J_2 . Atchison and Peck show in [18] that solar pressure and the Earth's oblateness are the dominant effects for high area-to-mass ratio spacecraft in orbits above LEO with the next strongest perturbative force, the third body effects of the Moon and the Sun, orders of magnitude smaller. The propagation does not take into account the effect of eclipses. Previous work has shown that this effect is small [17]. The model does not include aerodynamic drag. Instead a successful deorbit is defined as reaching a perigee altitude of below 100 km. The application of

drag is likely to slightly improve results as has been shown in previous work [12].

In three dimensions the angle ϕ is redefined as:

$$\phi = \Omega + \omega - (\lambda_{\odot} - \pi) \quad (8)$$

where Ω is the right ascension of the ascending node, ω is the argument of perigee and λ_{\odot} defines the position of the Sun on the ecliptic with respect to the vernal equinox as also shown in Figure 3. It has been shown that orbits with low inclination evolve in patterns similar to the behaviour described by the Hamiltonian in the planar case when observed in the orbital element phase space of eccentricity and ϕ as defined in Eq. (8) [13].

4.2. Equatorial circular orbits

When deorbiting circular, equatorial orbits the initial right ascension of the ascending node Ω_0 and the initial argument of perigee ω_0 are irrelevant. However, the initial position of the Sun $\lambda_{\odot,0}$ influences the orbital evolution. To account for this, the required effective area-to-mass ratios are found for a range of λ_{\odot} for each semi-major axis. To determine the required effective area-to-mass ratios to deorbit within a certain time limit, a stepwise search is performed. Starting with the analytical result obtained from Eqs. (5) and (6) the orbit is propagated for a given amount of time or until the criterion for deorbit is fulfilled. Depending on the result of the propagation a new value for the effective area-to-mass ratio is chosen. If the searched value lies between the last two steps the step size is halved. This is continued until a minimum step size is reached and thus the effective area-to-mass ratio can be determined with the required accuracy. The maximum deorbiting time is chosen as five years.

Figure 8 shows the maximum, minimum and mean relative error between the numerical and the analytical results. The mean required effective area-to-mass ratio is around 5% higher than previously estimated. The maximum overall relative error is 14% and occurs at geostationary altitude. The maximum error increases with altitude because the effects of solar radiation pressure dominate over the Earth's oblateness for higher orbits, and while in the analytical model the

orbit is considered equatorial with respect to the J_2 effect, it is considered to be in the ecliptic with respect to solar radiation pressure.

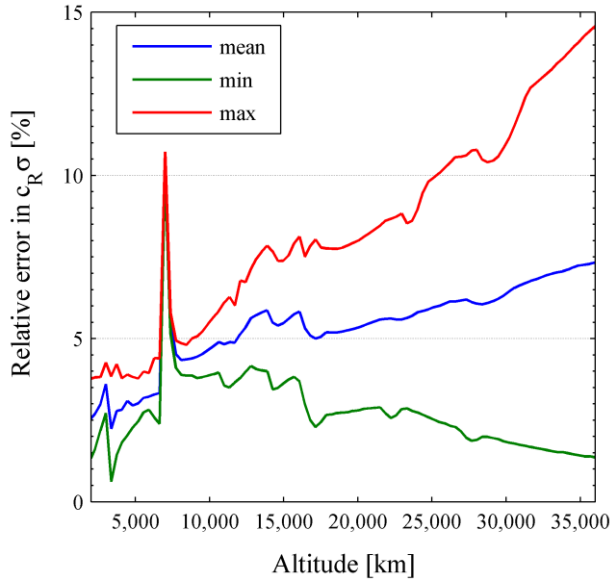


Figure 8: Relative error between analytical results in 2D and numerical results in 3D limited to a five year deorbiting manoeuvre.

4.3. Inclined circular orbits

For circular inclined orbits, apart from the initial position of the Sun $\lambda_{\odot,0}$, the initial right ascension of the ascending node Ω_0 is of importance. In this subsection the results for the required effective area-to-mass ratios to deorbit circular orbits of a range of inclinations and semi-major axes and the sensitivity towards initial orbit orientation $(\Omega_0, \lambda_{\odot,0})$ are presented and discussed.

The results were obtained in the same way as described in the previous section and saved in a four-dimensional array of initial semi-major axis, inclination, right ascension of the ascending node and solar angle.

Figure 9 shows the results for four selected semi-major axes. The required effective area-to-mass ratio is plotted over inclination for eight different Ω_0 identified by colour and four different λ_{\odot} identified by line style. The values for $\lambda_{\odot,0}$ range only from $[0, \pi]$ as both halves of the solution space are symmetrical. It can be seen that for the lower altitudes there is a decrease of required effective area-to-mass ratio with inclination until a minimum is reached. After this the required effective area-to-mass ratio increases again

and the results disperse, showing a higher sensitivity towards initial orientation. At 15,000 km the average required effective area-to-mass ratio increases with inclination while the sensitivity also increases. At 35,586 km i.e. geostationary altitude the average required effective area-to-mass ratio increases slightly with inclination. The sensitivity, however, strongly increases.

An explanation for the observed behaviour can be found in [13] where the extension of the stationary points in the (e, ϕ) phase space was investigated for non-zero obliquity of the ecliptic over the equator and non-zero inclinations. In the three dimensional SRP and J_2 dynamics an exact solution for equilibrium points does not exist; however, conditions for inclined quasi-frozen orbit can be found. Also in this case the quasi-stationary points of the phase space represent Sun-pointing apogee orbits ($\phi = \pi$) or Sun-pointing perigee orbits ($\phi = 0$). The reason for the improvement of the deorbit results in the 3D case for lower altitudes is that the eccentricity e_0 of the quasi-frozen point at $\phi = 0$, around which the lower altitude orbits librate, increases when the inclination is greater than zero [13]. However, both quasi-equilibria are only true equilibria in the planar case (zero obliquity and zero inclination). They become increasingly unstable with higher inclination and eventually disappear completely. This is the reason for the increase of required effective area-to-mass ratio after the initial drop. The eccentricity e_π of the quasi-frozen point at $\phi = \pi$, around which higher altitude orbits librate, decreases with increasing inclination. This explains why higher altitude orbits require an increasing effective area-to-mass ratio for larger inclinations.

Figure 10 shows the mean required effective area-to-mass ratio to deorbit a spacecraft from a circular orbit as a contour plot of initial semi-major axis and inclination.

While many of the values are very high and not feasible for near-term missions, a region can be identified spanning from 2,000 km altitude and about 40 degrees of inclination to about 7,500 km altitude and 0 degrees of inclination. In this region the required effective area-to-mass ratio to deorbit is lower than $10 \text{ m}^2/\text{kg}$ and can be as low as $1.2 \text{ m}^2/\text{kg}$. Figure 11 shows a higher resolution close-up of this region and the effective area-to-mass ratio requirements.

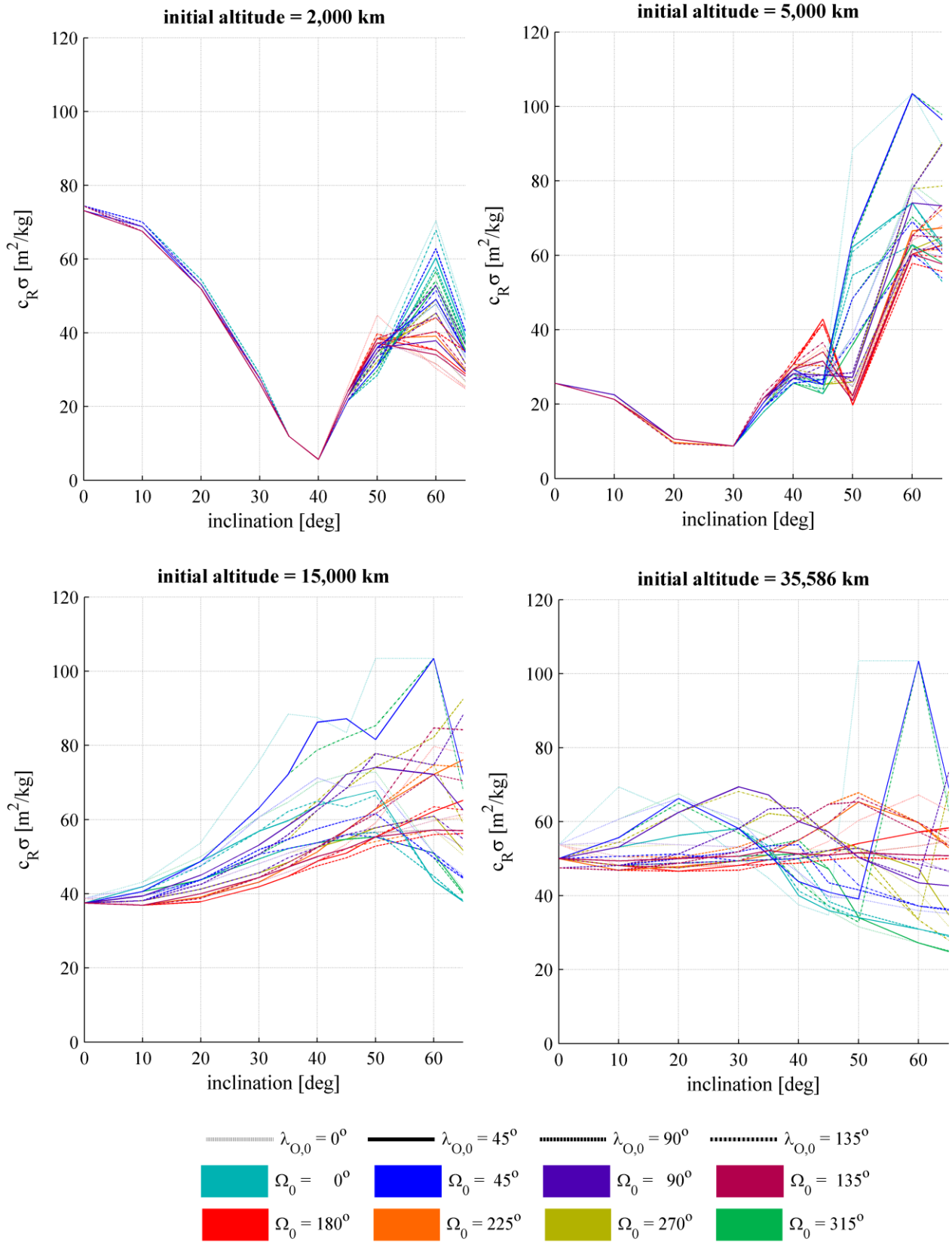


Figure 9: Numerical results for the required effective area-to-mass ratios to deorbit from an initially circular orbit

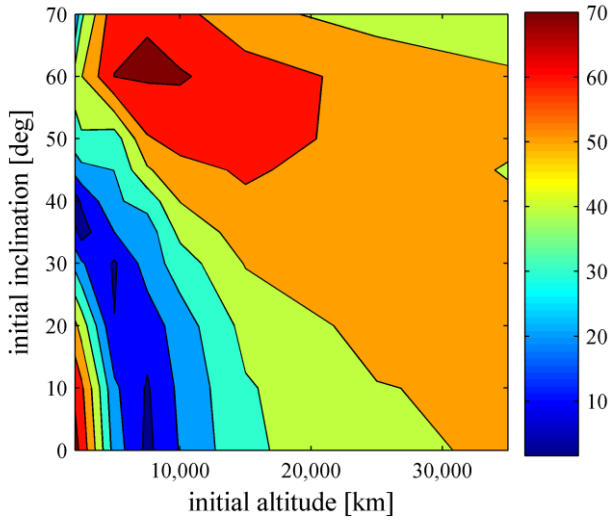


Figure 10: Mean required effective area-to-mass ratio to deorbit [m^2/kg].

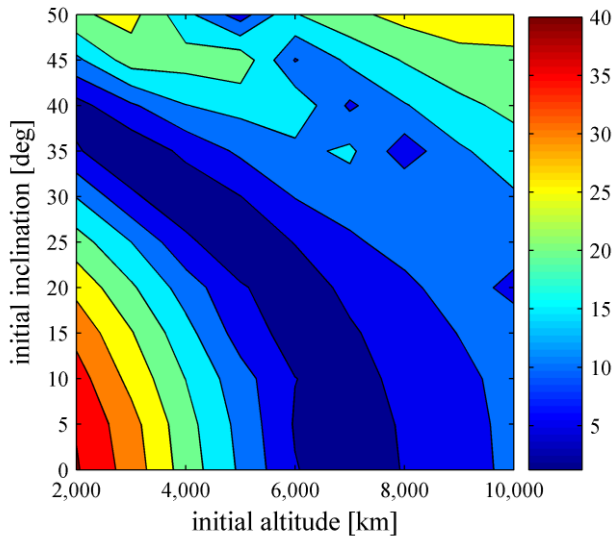


Figure 11: Required effective area-to-mass ratio to deorbit [m^2/kg]. Close-up of the low requirements region.

Figure 12 shows the standard deviation of all values calculated for the effective area-to-mass ratio at a given semi-major axis and inclination with respect to the initial right ascension of the ascending node and the initial position of the Sun. The results are the ones shown in Figure 9. The simulation was run for four different initial $\lambda_{\odot,0}$ and eight different initial Ω_0 . The standard deviation of these results can be seen as an indicator of sensitivity towards these two parameters which determine the initial orientation with respect to the Sun. This sensitivity is low for small inclinations and low altitudes.

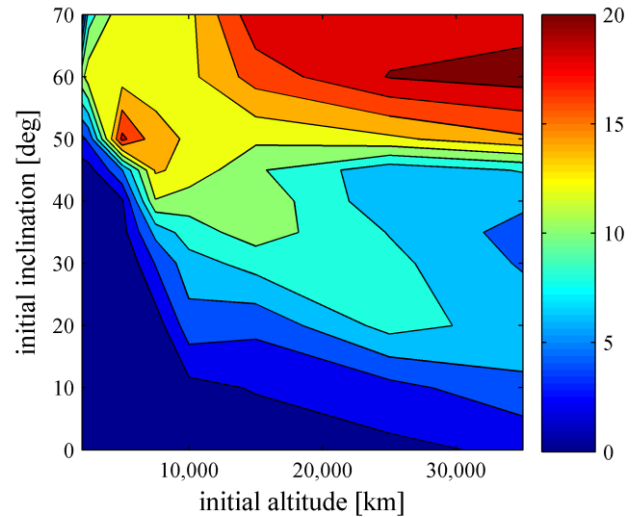


Figure 12: Standard deviation of the required effective area-to-mass ratio [m^2/kg] to deorbit with respect to the initial right ascension of the ascending node and initial position of the Sun on the ecliptic.

4.4. Eccentric orbits

The effective area-to-mass ratio to deorbit an eccentric orbit is dependant on six parameters: the initial eccentricity, semi-major axis, inclination, argument of perigee, right ascension of the ascending node and position of the Sun on the elliptic. In order to narrow this down, only one type of eccentric orbit is investigated here, the Molniya orbit. This orbit is one of the most common eccentric orbits. It has the critical inclination of 63.4 degrees to avoid a drift in argument of perigee due to the J_2 effect [19]. Its orbital period is half a nodal day to achieve a repeat ground track and the fixed argument of perigee is usually -90 degrees to offer long coverage of the high latitude regions of the northern hemisphere. The perigee altitude is at around 600 km and the semi-major axis is about 26,500 km. The most common spacecraft group in eccentric MEO orbits as identified in Section 2 are the spacecraft of the Oko constellations. These were originally launched into Molniya orbits but drifted from their original orbits after the end-of-operations. Molniya orbits experience strong third body perturbations from the Moon and the Sun which cause the eccentricity to change over time [20].

With the eccentricity, semi-major axis, inclination and argument of perigee given for a Molniya orbit, the variable parameters are the initial right ascension of the ascending node and the initial position of the Sun on the ecliptic. Simulation results show that the angle between the direction of the Sun and the right

ascension of the ascending node is the determining factor for the required effective area-to-mass ratio. Deorbiting is only feasible in the range of $0 < \Omega_0 - \lambda_{\odot,0} < 90^\circ$. That means that while any Molniya satellites can be deorbited using solar radiation pressure and J_2 , depending on its initial orientation only the manoeuvre can only be initiated at a certain time in the year.

Figure 13 shows the results for different initial positions of the Sun $\lambda_{\odot,0}$. Outside the feasible zone, of the sensitivity with respect to initial solar orientation increases dramatically while it is very low at $\Omega_0 - \lambda_{\odot,0} = 90^\circ \pm 45^\circ$. Here the required effective area-to-mass ratio is just $1 \text{ m}^2/\text{kg}$. A 1,000 kg satellite needs to deploy a circular, reflective sail with 13 meters radius to achieve this requirement.

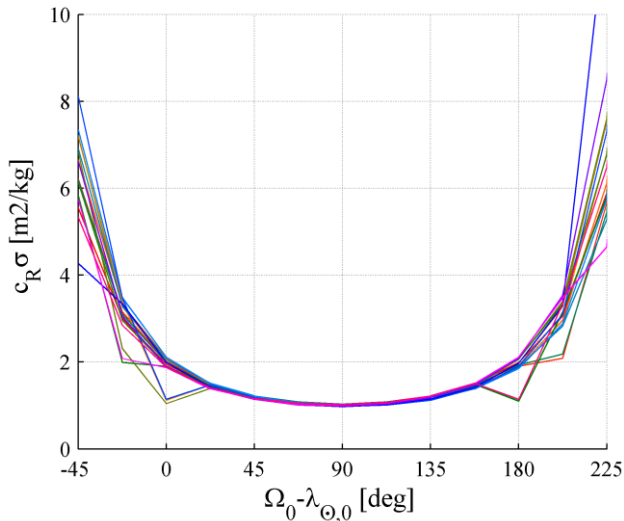


Figure 13: Required effective area-to-mass ratio to deorbit a spacecraft in a Molniya for different initial λ_{\odot} as a function of the angle between right ascension of the ascending node and the position of the Sun on the ecliptic.

5. CONCLUSIONS

This paper investigates the applicability of passive deorbiting using the effects of solar radiation pressure and the Earth's oblateness to MEO spacecraft. This method was previously presented for a planar case using an analytical approximation.

It has been shown that the analytical planar results translate into the three dimensional space for equatorial orbits. The required effective area-to-mass ratio to deorbit circular orbits changes with inclination and its

sensitivity with respect to initial orientation increases. There is a region in the inclination and semi-major axis parameter space in which deorbiting is very feasible with required area-to-mass ratios of below $10 \text{ m}^2/\text{kg}$.

Looking back at the survey of current MEO objects presented in Section 2, the important regions identified in this section can be assessed for deorbiting with the method presented in this paper. GNSS satellites in high inclination orbits of around 20,000 km altitude and below-GEO orbits with low inclination and around 34,000 km altitude are not suitable for deorbiting with solar radiation pressure and the J_2 effect only as the required effective area-to-mass ratios would be in the region of $50 \text{ m}^2/\text{kg}$. However, Molniya orbits can be deorbited with an effective area-to-mass ratio of just $1 \text{ m}^2/\text{kg}$.

The method could also be of interest to future high altitude small satellite missions. For example a 3U CubeSat in a 3,000 km altitude orbit with 40 degrees of inclination can be deorbited with a circular, reflective device of less than 80 cm radius.

ACKNOWLEDGMENTS

This work was funded by the European Research Council grant 227571 (VISIONSPACE).

Charlotte Lücking is also supported by the IET Hudswell International Scholarship 2011 and the Frank J. Redd Student Scholarship.

REFERENCES

- [1] IADC. "IADC Space Debris Mitigation Guidelines." 2002.
- [2] Johnson, N. L. "Medium Earth Orbits: is there a need for a third protected region?," *61st International Astronautical Congress*. Prague, CZ, 2010.
- [3] European Commission, "Commission presents midterm review of European satellite navigation programmes Galileo and EGNOS". Brussels, 18.01.2011
- [4] Roberts, P. C. E., and Harkness, P. G. "Drag Sail for End-of-Life Disposal from Low Earth Orbit," *Journal of Spacecraft and Rockets* Vol. 44, No. 6, 2007, p. 9.
doi: 10.2514/1.28626

- [5] Maessen, D. C., Breukelen, E. D. v., Zandbergen, B. T. C., and Bergsma, O. K. "Development of a Generic Inflatable De-orbit Device for CubeSats," *58th International Astronautical Congress*. 2007.
- [6] Nock, K. T., Gates, K. L., Aaron, K. M., and McDonald, A. D. "Gossamer Orbit Lowering Device (GOLD) for Safe and Efficient De-orbit," *AIAA Astrodynamics Specialists Conference*. Toronto, Canada, 2010.
- [7] Andrews, J., Watry, K., and Brown, K. "Nanosat Deorbit and Recovery System to Enable New Missions," *25th Annual AIAA/USU Conference on Small Satellites*. Logan, Utah, USA, 2011.
- [8] Iess, L., Bruno, C., Olivieri, C., Ponzi, U., Parisse, M., Laneve, G., Vannaroni, G., Dobrowolny, M., De Venuto, F., Bertotti, B., and Anselmo, L. "Satellite de-orbiting by means of electrodynamic tethers part I: General concepts and requirements," *Acta Astronautica* Vol. 50, No. Compendex, 2002, pp. 399-406.
- [9] Iess, L., Bruno, C., Olivieri, C., and Vannaroni, G. "Satellite de-orbiting by means of electrodynamic tethers part II: System configuration and performance," *Acta Astronautica* Vol. 50, No. Compendex, 2002, pp. 407-416.
- [10] Hoyt, R. P., Barnes, I. M., Voronka, N. R., and Slostad, J. T. "The Terminator Tape: A cost-effective de-orbit module for end-of-life disposal of LEO satellites," *AIAA Space 2009 Conference and Exposition, September 14, 2009 - September 17, 2009*. American Institute of Aeronautics and Astronautics Inc., Pasadena, CA, United states, 2009.
- [11] Lücking, C., Colombo, C., and McInnes, C. R. "A Passive De-orbiting Strategy for High Altitude CubeSat Missions using a Deployable Reflective Balloon," *8th IAA Symposium on Small Satellites for Earth Observation*. Berlin, Germany, 2011.
- [12] Lücking, C. "A Passive High Altitude Deorbiting Strategy," *25th AIAA/USU Conference on Small Satellites*. Logan, Utah, USA, 2011.
- [13] Colombo, C., Lücking, C., and McInnes, C. R. "Orbital Dynamics of High Area-to-Mass Ratio Spacecraft under the Influence of J_2 and Solar Radiation Pressure," *62nd International Astronautical Congress*. Cape Town, 2011.
- [14] Podvig, P. "History and the Current Status of the Russian Early-Warning System," *Science and Global Security* Vol. 10, 2002, p. 21:60.
doi: 10.1080/08929880290008395
- [15] Shapiro, I. I., Jones, H. M., and Perkins, C. W. "Orbital properties of the West Ford dipole belt," *Proceedings of the IEEE* Vol. 52, No. 5, 1964, pp. 469-518.
- [16] Krivov, A. V., and Getino, J. "Orbital evolution of high-altitude balloon satellites," *Astronomy and Astrophysics* Vol. 318, 1997, pp. 308-314.
- [17] Krivov, A. V., Sokolov, L. L., and Dikarev, V. V. "Dynamics of Mars-orbiting dust: Effects of light pressure and planetary oblateness," *Celestial Mechanics and Dynamical Astronomy* Vol. 63, No. 3, 1995, pp. 313-339.
doi: 10.1007/bf00692293
- [18] Atchison, J. A., and Peck, M. A. "Length Scaling in Spacecraft Dynamics," *Journal of guidance, control, and dynamics* Vol. 34, No. 1, 2011, pp. 231-246.
doi: 10.2514/1.49383
- [19] Kidder, S. Q., and Haar, T. H. V. "On the use of satellites in Molniya orbits for meteorological observation of middle and high latitudes," *Journal of Atmospheric and Oceanic Technology* Vol. 7, 1990, pp. 517-522.
doi: 10.1175/1520-0426(1990)007<0517:OUTOSI>2.0.CO;2
- [20] Kolyuka, Y. F., Ivanov, N. M., Afanasieva, T. I., and Gridchina, T. A. "Orbit Evolution and Uncontrolled Re-entry of the "Molniya" Type Satellites," *Fifth European Conference on Space Debris*. Darmstadt, Germany, 2009.